research papers

Fingerprinting redox and ligand states in haemprotein crystal structures using resonance Raman spectroscopy

Demet Kekilli,[a] Florian S. N. Dworkowski,[b] Guillaume Pompidor,[b]‡ Martin R. Fuchs,[b]§ Colin R. Andrew,[c] Svetlana Antonyuk,[d] Richard W. Strange,[d] Robert R. Eady,[d] S. Samar Hasnain[d] and Michael A. Hough[a]*

[a]School of Biological Sciences, University of Essex, Wivenhoe Park, Colchester CO4 3SQ, England, [b]Swiss Light Source, Paul Scherrer Institut, CH-5232 Villigen PSI, Switzerland, [c]Department of Chemistry and Biochemistry, Eastern Oregon University, La Grande, OR 97850-2899, USA, and [d]Institute of Integrative Biology, Faculty of Health and Life Sciences, University of Liverpool, Crown Street, Liverpool L69 7ZB, England

‡ Current address: European Molecular Biology Laboratory Hamburg c/o DESY, Notkestrasse 85, D-22603 Hamburg, Germany.
§ Current address: Department of Photon Sciences, Brookhaven National Laboratory, Upton, NY 11973, USA.

Correspondence e-mail: mahough@essex.ac.uk

It is crucial to assign the correct redox and ligand states to crystal structures of proteins with an active redox centre to gain valid functional information and prevent the misinterpretation of structures. Single-crystal spectroscopies, particularly when applied *in situ* at macromolecular crystallography beamlines, allow spectroscopic investigations of redox and ligand states and the identification of reaction intermediates in protein crystals during the collection of structural data. Single-crystal resonance Raman spectroscopy was carried out in combination with macromolecular crystallography on Swiss Light Source beamline X10SA using cytochrome c' from *Alcaligenes xylosoxidans*. This allowed the fingerprinting and validation of different redox and ligand states, identification of vibrational modes and identification of intermediates together with monitoring of radiation-induced changes. This combined approach provides a powerful tool to obtain complementary data and correctly assign the true oxidation and ligand state(s) in redox-protein crystals.

1. Introduction

It is essential that crystal structures of metalloproteins are assigned to the correct redox and ligand states in order to gain maximum functional information and to avoid, for example, the misinterpretation of catalytic mechanisms. In the case of haemproteins that bind small gaseous ligands, the ability to identify the nature and occupancy of a ligand where there may be limited differences in electron density is crucial. Recent developments in single-crystal micro-spectrophotometry, particularly when applied *in situ* on synchrotron macromolecular crystallography beamlines, allow systematic spectroscopic monitoring of redox and ligand states in the crystals that are used for structure determination. This enables identification of the initial state of the crystal and its comparison with solution data and also the ability to monitor changes induced by X-ray irradiation.

The application of UV–visible spectroscopy to protein single crystals has become well developed in recent years (Pearson & Owen, 2009; Pearson *et al.*, 2007; Owen *et al.*, 2011; Orville *et al.*, 2011; Ellis *et al.*, 2008; Antonyuk & Hough, 2011), while a number of beamlines, including those at the ESRF, NSLS (Stoner-Ma *et al.*, 2011) and Swiss Light Source (SLS; Pompidor *et al.*, 2013), also now have the capability to conduct Raman spectroscopy either in non-resonance (Carpentier *et al.*, 2007; Katona *et al.*, 2007; Bourgeois *et al.*, 2009) or resonance (RR; Daughtry *et al.*, 2012) modes. The preferred goal is to measure data from the X-ray-exposed portion of the same crystal from which the crystal structure is determined. Recent developments of the on-axis multi-mode

microspectrophotometer (Pompidor *et al.*, 2013) at beamline X10SA of the SLS allow back-scattered resonance Raman (RR) data to be conveniently measured along the same axis as the X-ray beam (ensuring good alignment) with minimal or no impact on the efficiency of crystallographic data collection.

The gas-binding haemprotein cytochrome c' from the denitrifying bacterium *Alcaligenes xylosoxidans* (*Ax*CYTcp) discriminates between nitric oxide (NO) and carbon monoxide (CO) by binding them to opposite faces of haem while excluding the binding of molecular oxygen. In the absence of gaseous ligands, the haem Fe ion is five-coordinate (5c) with a proximal histidine ligand and a vacant distal coordination site. CO binds at the distal face to form a six-coordinate (6c) adduct, while NO initially forms a 6c distal NO adduct and proceeds *via* a transient dinitrosyl intermediate to form the stable 5c proximal adduct, involving displacement of

the proximal histidine (Andrew *et al.*, 2002; Lawson *et al.*, 2000). The 6c-to-5c conversion of NO ligation in cytochrome c' has recently been confirmed to be highly relevant to the mechanism of activation of soluble guanylate cyclase (Martin *et al.*, 2012; Tsai *et al.*, 2011), and proximal NO binding also occurs in the pro-apoptotic cytochrome *c*–cardiolipin complex (Silkstone *et al.*, 2012). In neither of these cases are structural data available and *Ax*CYTcp provides a valuable structural model for NO binding.

Detailed solution RR studies have been performed on *Ax*CYTcp (Andrew *et al.*, 2001, 2002, 2005; Kruglik *et al.*, 2007) and on a number of site-directed mutants (Antonyuk *et al.*, 2011; Hough *et al.*, 2011; Garton *et al.*, 2012). High-resolution crystallographic analysis (Lawson *et al.*, 2000; Antonyuk *et al.*, 2011; Hough *et al.*, 2011) of this protein and its mutants has provided detailed structural information, yet correlating crystallographic and solution spectroscopic data has remained a considerable challenge. The large irradiated surface area and very high resolution diffraction of *Ax*CYTcp crystals, together with the wealth of comparative solution data, make this protein an ideal test candidate for combined RR and crystallographic methods.

In this study, we present a comprehensive, correlated single-crystal RR and structural study of *Ax*CYTcp in its ferric, ferrous and gas ligand-bound forms as well as characterizing X-ray-induced changes to these states. We demonstrate that redox and ligand states in crystal structures can be effectively spectroscopically fingerprinted *in situ* on the macromolecular crystallography beamline X10SA. This approach, if applied routinely to structural studies of haemproteins, has the potential to radically increase and complement the biological significance of the results gained from crystallographic experiments, such as redox-dependent biological mechanisms.
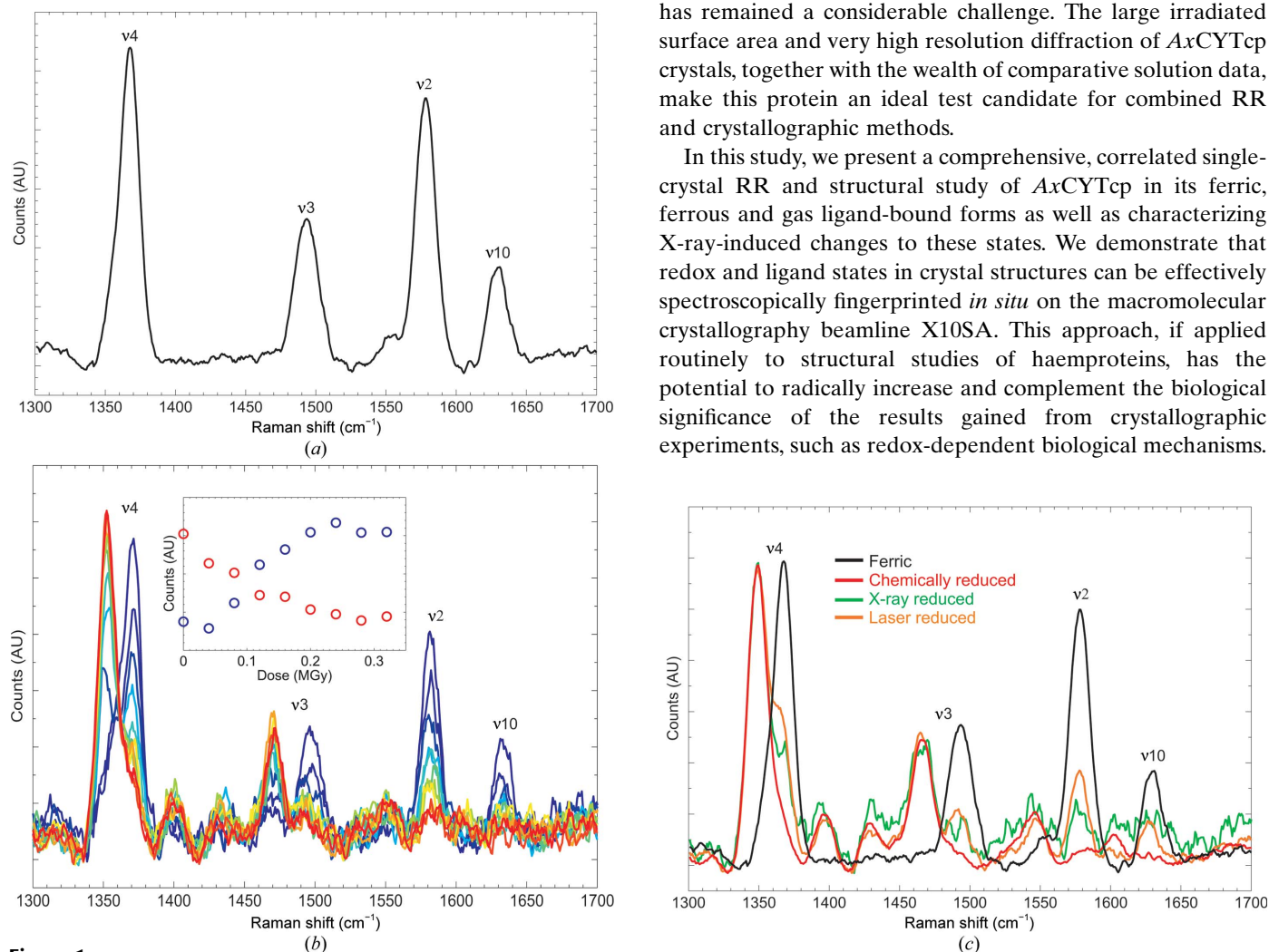
Figure 1
(*a*) RR spectra measured from a ferric *Ax*CYTcp crystal at 100 K. The redox marker ν_4 and the core size markers ν_3, ν_2 and ν_{10} are clearly defined. (*b*) X-ray-reduction kinetic series of 20 s RR measurements. The first spectrum is shown in blue, with reduction essentially complete after an absorbed X-ray dose of ∼0.19 MGy. The inset shows the dose-dependent change in the bands at 1371 cm^{-1} (red) and 1352 cm^{-1} (blue). (*c*) RR spectra of ferric, chemically reduced, laser-reduced and X-ray-reduced crystals. Several spectra for each state were measured before X-ray exposure to ensure that no laser effects were apparent (except for the laser-reduced data) and only a single spectrum for each state is presented here. Data from a ferric crystal (black) were measured over 30 s at ∼2 mW, data from an X-ray-reduced crystal (green) over 20 s at ∼0.88 mW and data from a chemically reduced crystal (red) over 30 s at ∼2 mW. The laser-reduced spectrum shown (orange) was the final spectrum of a series of 20 × 30 s at ∼4.8 mW. Raman shifts measured from all three ferrous crystals are consistent within experimental error with solution data for the ferrous form of *Ax*CYTcp (Table 1).

Table 1
High-frequency Raman shifts (cm^{-1}) measured from crystals of AxCYTcp and comparative solution data at 100 K.

n.o., not observed.

State	T (K)	Excitation λ (nm)	ν_4	ν_3	ν_2	ν_{10}	Reference
Ferric solution	100	413.1	1370	1493	1581	1630	C. R. Andrew (unpublished data)
Ferric crystal	100	405.4	1369	1492	1577	1630	This work
Chemically reduced crystal	100	405.4	1350	1467	1582	1602	This work
X-ray-reduced crystal	100	405.4	1352	1466	n.o	n.o	This work
Laser-reduced crystal	100	405.4	1350	1467	1578	n.o	This work
Ferrous solution	90	413.1	1353	1471	1579	1607	Andrew et al. (2002)
NO-bound solution	90	413.1	1375	1504	1596	1638	Andrew et al. (2002)
NO-bound crystal	100	405.4	1378	1512	1597	1648	This work
CO-bound solution	100	413.1	1370	—	1597	1634	Antonyuk et al. (2011)
CO-bound crystal	100	405.4	1369	—	1598	—	This work

2. Materials and methods

Recombinant native AxCYTcp was expressed and purified and crystals were grown as described previously (Hough et al., 2011; Antonyuk et al., 2011). Crystals were transferred into a cryoprotectant solution consisting of 40% sucrose, 2.4 M ammonium sulfate, 100 mM HEPES buffer pH 7.5 for 10 s before flash-cooling in liquid nitrogen. To generate the ferrous state, ferric crystals were transferred into ~2 ml deoxygenated mother-liquor solution containing 100 mM ascorbate within a sealed glass bottle for ~2 h. Ligand-bound states were produced from ferrous crystals either via bubbling of CO gas through the liquid for ~5 min or injection of 10 µl of a stock solution of the NO-donor compound ProliNONOate (Cayman Chemical; Saavedra et al., 1996) in 25 mM NaOH into the solution.

All crystallographic data were measured on SLS beamline X10SA using a PILATUS 6M-F detector (Dectris; Henrich et al., 2009). Data were processed using XDS (Kabsch, 2010) and SCALA (Evans, 2006) in the CCP4 (Winn et al., 2011) suite. The structures were refined using REFMAC5 (Murshudov et al., 2011) using the most appropriate structures of AxCYTcp from the Protein Data Bank as the starting models. Anisotropic temperature factors were refined where the resolution allowed, and riding H atoms were added to the models. Model building between cycles of refinement was performed in Coot (Emsley et al., 2010), and the quality of the structure was monitored using MolProbity (Chen et al., 2010) and JCSG Quality Control Check v.3.0. Measurements at elevated cryogenic temperatures were obtained by varying the Cryojet temperature setting. Data-collection and refinement statistics are given in Supplementary Tables S1 and S2.[1] Coordinates and structure factors have been deposited in the RCSB Protein Data Bank with the accession codes given in Supplementary Table S1.

Single-crystal RR data were measured on beamline X10SA from the same crystals immediately preceding or following X-ray diffraction measurements. The on-axis multi-mode microspectrophotometer versions MS2 (Pompidor et al., 2013) and MS3 (Dworkowski et al., in preparation) were used with a solid-state excitation laser (Omicron Laserage LDM405, 400, CWA) wavelength of 405.4 nm. The Andor Shamrock 303i spectrograph used a 2400 l mm^{-1} grating, blazed at 300 nm. Spectra were measured using an ANDOR Newton EM-CCD DU-970N-UVB (1600 × 200 pixels; Andor Technology PLC, Belfast, Northern Ireland) cooled to 193 K in full vertical binning mode. Raman shifts were calibrated using cyclohexane or 4-acetamidophenol as a reference. Laser powers at the sample position were measured using a PMD100D hand-held power meter (Thorlabs Inc., New Jersey, USA). All spectra were processed and background-subtracted using the in-house SLS-APE analysis toolbox (Dworkowski et al., manuscript in preparation). Absorbed X-ray doses were calculated using the program RADDOSE-3D (Zeldin et al., 2013).

3. Results

3.1. Measurement of resonance Raman data from AxCYTcp crystals and monitoring of X-ray-reduction effects

Resonance Raman (RR) data over the wavenumber range 600–2000 cm^{-1} were measured from native ferric AxCYTcp crystals using 405.4 nm laser excitation and on-axis geometry[2] (Fig. 1 and Supplementary Fig. S1). The spectra showed good signal to noise, allowing a large number of Raman shifts to be detected characteristic of haem porphyrin groups. The spectrum measured from a ferric AxCYTcp crystal was consistent with equivalent solution data measured at 100 K (Table 1). Raman shifts in the haem porphyrin marker region are shown in Fig. 1(a) and Table 1. The values for the redox-state marker ν_4 and the haem core size markers ν_3 and ν_{10} lie within 1 cm^{-1} of those measured in solution, while the remaining core size marker ν_2 is shifted by 4 cm^{-1} in the crystal data. These small differences are similar to the inherent resolution of the instrumentation (~3 cm^{-1}), but may also represent differences owing to the protein being in either a crystal lattice or in the solution state. Raman spectra taken from several different crystals of ferric AxCYTcp on separate visits to the beamline gave values for the porphyrin marker bands that were reproducible between 2–3 cm^{-1} (data not shown). Laser powers at the sample position[3] were chosen below the threshold at which laser-induced photoreduction of the ferric haem is observed (<2.4 mW; Dworkowski et al., in preparation[4]). Where appropriate, at least two consecutive

---

[1] Supporting information has been deposited in the IUCr electronic archive (Reference: TZ5051).

[2] Note that the laser light (405.4 nm) penetrates only a few micrometres into the crystal. An off-axis geometry without crystal reorientation would therefore not fully sample the X-ray-irradiated area.

[3] Laser powers given are those measured at the sample position unless otherwise noted.

[4] Note that for the laser spot size used, power densities are between 0.45 mW mm^{-2} (for 0.88 mW power) and 2.45 mW mm^{-2} (4.8 mW laser power).

RR spectra in the absence of X-rays were taken for each measurement in order to exclude laser-induced effects on the crystals.

To investigate X-ray reduction of the ferric haem in *Ax*CYTcp crystals, a kinetic series of 50 RR spectra, each of 20 s laser exposure, were measured using a laser power of 0.88 mW. A 'blank' kinetic series measured first confirmed that no laser-induced spectral changes were evident before the X-ray shutter was opened. Upon X-ray irradiation, the spectrum of ferric haem was rapidly interconverted to a spectrum with well resolved bands at 1352 and 1466 cm^{-1} (Fig. 1b, Table 1) corresponding to the ferrous protein. Complete conversion to the ferrous form was observed after a total absorbed X-ray dose of 0.19 MGy (0.024 MGy per spectrum;[5] Fig. 1b).

3.2. Measurement of a validated ferric haem crystal structure

Given that rapid X-ray-induced reduction of the *Ax*CYTcp haem iron(III) was observed, strategies were investigated to measure an 'intact' spectrum of the 'genuine' ferric form, and a multi-spot composite data-collection strategy was applied to large crystals (>1 mm maximum dimension) of ferric *Ax*CYTcp. This approach is analogous to that used to determine an intact state of an X-ray-sensitive ferryl intermediate in peroxidase (Meharenna *et al.*, 2010). Five different positions along the crystal were chosen and marked using the bookmarking feature of the data-collection GUI. Partial data sets, each comprising 8° crystal rotation, were measured, with the crystal translated to a new position between wedges. Rotation ranges at adjacent positions had a 2° overlap in order to allow accurate scaling.

A single RR spectrum was measured from the crystal prior to X-ray exposure and at each bookmarked crystal position following X-ray data collection to ensure that no observable photoreduction had occurred (Supplementary Fig. S2). Each RR spectrum was collected at the ω angle in the centre of the rotation range used for the corresponding diffraction data wedge. A total of 32 diffraction images were obtained at each of the five positions at an X-ray wavelength of 0.8 Å, an X-ray flux of 2.97×10^{10} photons s^{-1} and a beam size of 50 × 50 μm, which were processed and merged together to give a complete data set (Supplementary Table S1). With a highly attenuated X-ray beam the absorbed dose per data set was only 7.9 kGy. The resulting spectroscopically validated crystal structure for the ferric protein was determined to 1.3 Å resolution. The structure shows the Arg124 side chain in a position parallel to the haem as previously proposed for the ferric state (Lawson *et al.*, 2000). Structural parameters for the haem site of this and the other structures described herein are given in Table 2.

3.3. Comparison of crystals reduced chemically and by X-ray irradiation

Combined X-ray and RR data were measured from crystals reduced by different means: (i) chemical reduction using sodium ascorbate prior to crystal cooling, (ii) *in situ* reduction

Table 2
Resolution and haem-ligand parameters for spectroscopically correlated *Ax*CYTcp crystal structures.

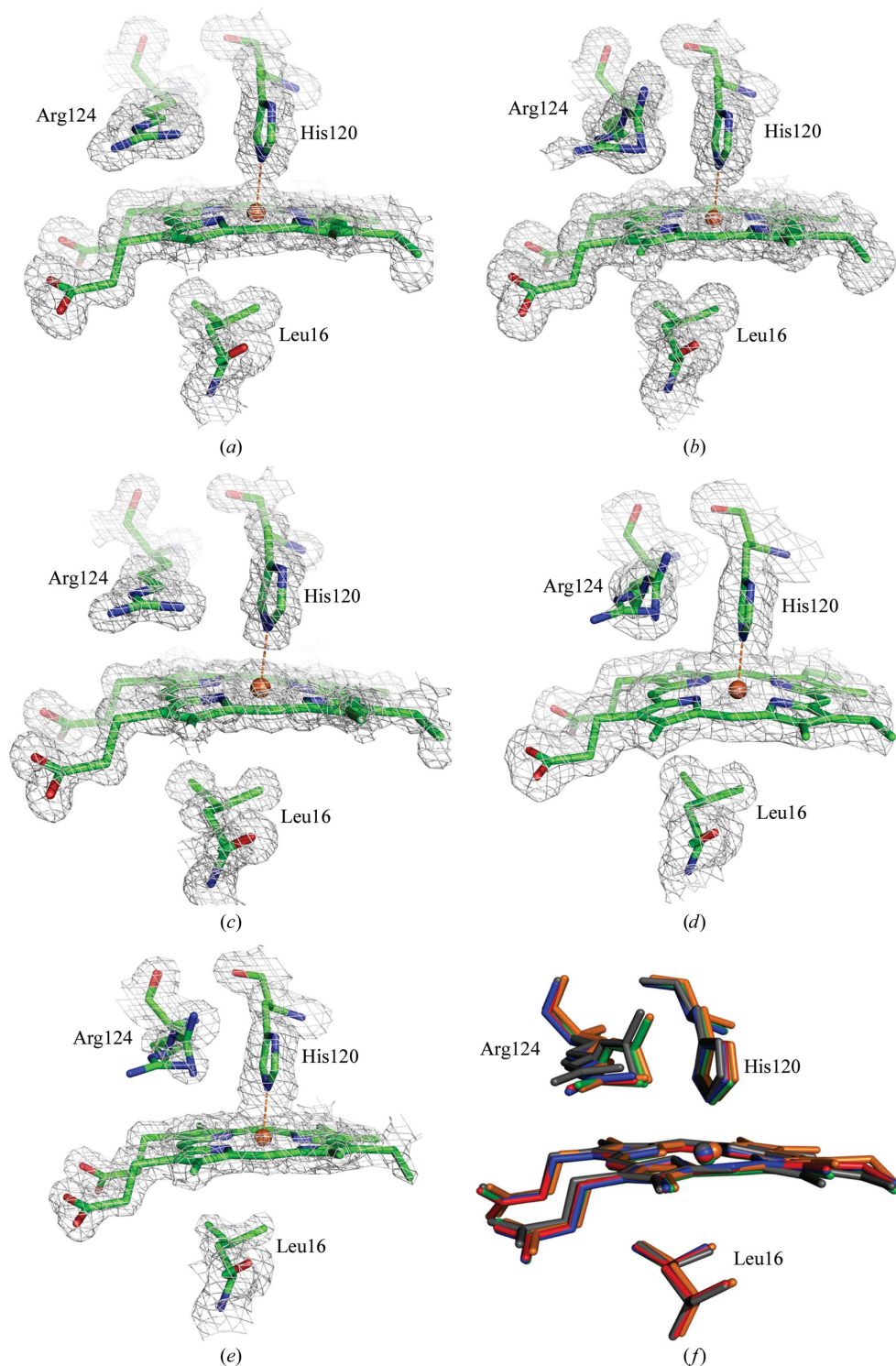| Structure	Resolution (Å)	Fe—His120 N (Å)	Fe—N (Å)	Fe—N—O angle (°)
Ferric	1.30	2.05	—	—
Chemically reduced	1.22	2.14	—	—
X-ray-reduced (100 K)	1.17	2.12	—	—
X-ray-reduced (160 K)	1.77	2.15	—	—
X-ray-reduced (180 K)	1.55	2.04	—	—
5c NO complex	1.26	—	1.84	42.1

by exposure to X-rays and (iii) reduction by exposure to a high-power (~4.8 mW) excitation laser (600 s exposure) as described in Dworkowski *et al.* (in preparation). All three approaches yield similar spectra and indicate reduction of the initial ferric haem in the crystal to the ferrous state (Fig. 1c), with similar frequencies to those previously measured in solution (Table 1). Crystal structures were determined from chemically reduced crystals together with a crystal that had been reduced by X-rays, with confirmatory RR data measured to ensure that no further changes had occurred during crystallographic data collection. Owing to the limited penetration depth of the excitation laser of only a few micrometres (Adar *et al.*, 2010), a crystal with a depth greater than this penetration depth cannot be fully laser-reduced. To avoid possible misinterpretation of a partially reduced state, we did not measure diffraction data from a laser-reduced sample.

The porphyrin RR frequencies of chemically reduced and X-ray-reduced crystals are similar (Table 1). Interestingly, chemically and X-ray-reduced *Ax*CYTcp structures show large structural differences in the vicinity of the haem (Fig. 2), including the orientation of Arg124, previously proposed as a marker for sensing the Fe redox state. The ascorbate-reduced structure (Fig. 2b) agrees with previously reported ferrous *Ax*CYTcp structures in which the Arg124 guanadinium group is oriented perpendicular to the haem. By contrast, the X-ray-reduced structure shows Arg124 parallel to the haem (Fig. 2c), in a similar orientation to the ferric state (Fig. 2a). We propose that the discrepancy between the chemically reduced and X-ray-reduced structures is owing to the low (100 K) temperature of the crystal, such that conformational rearrangements in the haem pocket following photoreduction of haem Fe are restricted. To investigate this phenomenon further, the X-ray reduction experiment was repeated using fresh crystals at the elevated cryogenic temperatures of 160 and 180 K. These temperatures are lower than those at which crystalline ice formation in the crystals occurs and thus good-quality diffraction data could still be obtained. As expected, the signal-to-noise of the RR data deteriorated rapidly as the temperature was increased, but reduction could still be monitored *via* the shift in the ν_4 band to 1350 cm^{-1}, although the other bands characteristic of the ferrous protein could not be detected above the noise level.[6]

---

[5] The values quoted are the 'threshold average dose' calculated in *RADDOSE*-3D (Zeldin *et al.*, 2013).

[6] Interestingly, however, the chemically reduced crystal showed a small proportion (occupancy 0.2) of Arg124 in the 'ferric' orientation, suggesting that reduction was not complete prior to freezing of the crystal.

The structure of *Ax*CYTcp reduced by X-rays at 160 K was determined to a resolution of 1.77 Å, and in sharp contrast to the data set measured at 100 K it displayed two conformations

of Arg124, with the minor one (occupancy 0.3) similar to that present in the ferric structure and the major one (occupancy 0.7) corresponding to that in the chemically reduced crystal (Fig. 2*b*), indicating that conformational rearrangements supressed at 100 K were able to occur at higher temperatures. Additional data measured at 180 K showed a similar structure, again with a predominant 'chemically reduced ferrous' orientation of this side chain (occupancy 0.7) evident with a small component (occupancy 0.3) of the 'ferric' orientation. A superposition of the haem environments for the ferric, ascorbate-reduced, X-ray-reduced (100 K), X-ray-reduced (160 K) and X-ray-reduced (180 K) structures is shown in Fig. 2(*f*). The Fe–His bond length was shortest (2.05 Å) in the composite ferric structure, becoming slightly longer in crystals reduced at 100 K (2.12 Å) or reduced using ascorbate (2.14 Å). In the structures determined at 160 and 180 K the values were 2.15 and 2.04 Å, respectively, which are essentially the same given the lower resolution of these higher temperature structures.

The structures determined at 160 and 180 K exhibited a higher level of general radiation damage (beyond the haem pocket) than was the case at 100 K. While no disulfide bonds are present in *Ax*CYTcp, decarboxylation and loss of side-chain electron density were very evident in the higher temperature structures. The unit cell underwent a small expansion at higher temperature, with an increase of ∼0.3 Å in *a* and *b* and ∼1.0 Å in *c* between 100 and 160 K, while no further change was apparent between 160 and 180 K.

Figure 2
$2F_o - F_c$ electron-density maps contoured at 1σ showing the *Ax*CYTcp crystal structures of (*a*) ferric, (*b*) chemically reduced and (*c*) X-ray-reduced forms at 100 K. Additional X-ray-reduced structures determined at different temperatures are shown at 160 K (*d*) and 180 K (*e*). (*f*) Superposition of X-ray-reduced structures determined at 100 K (red), 160 K (grey) and 180 K (orange) with those of the chemically reduced (green) and ferric (blue) crystals. Note that in the chemically reduced, 160 and 180 K structures a minor occupancy conformation of Arg124 is present with density below the 1σ level (see Supplementary Fig. S3).

3.4. Monitoring of gas ligand-bound states

Data were measured from *Ax*CYTcp crystals that had been chemically reduced with sodium

ascorbate and exposed to either NO or CO prior to cooling to 100 K (Fig. 3). The CO-bound crystal exhibits porphyrin RR characteristic of a 6c low-spin species: ν_4 (1369 cm^{-1}) and ν_2 (1598 cm^{-1}), with ν_3 and ν_{10} modes not observed owing to low intensity. The RR spectrum for the NO-bound crystal is characteristic of a 5c NO haem with porphyrin marker bands ν_4 (1378 cm^{-1}), ν_3 (1512 cm^{-1}), ν_2 (1597 cm^{-1}) and ν_{10} (1648 cm^{-1}) (Table 1). The ν_4 and ν_2 frequencies of the 6c CO and 5c NO crystals at 100 K are similar to those of frozen solutions (100 K), although the ν_3 and ν_{10} frequencies of the 5c
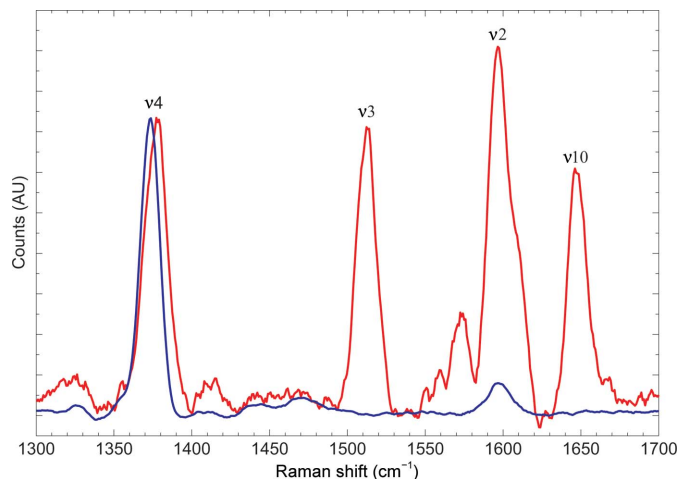
Figure 3
RR spectra measured from CO-bound (blue) and NO-bound (red) AxCYTcp crystals. The sample laser power was 1.95 mW with 70 s exposures. The spectra show characteristic frequencies for 6c (CO) and 5c (NO) complexes, respectively, and a comparison with solution data is given in Table 1.
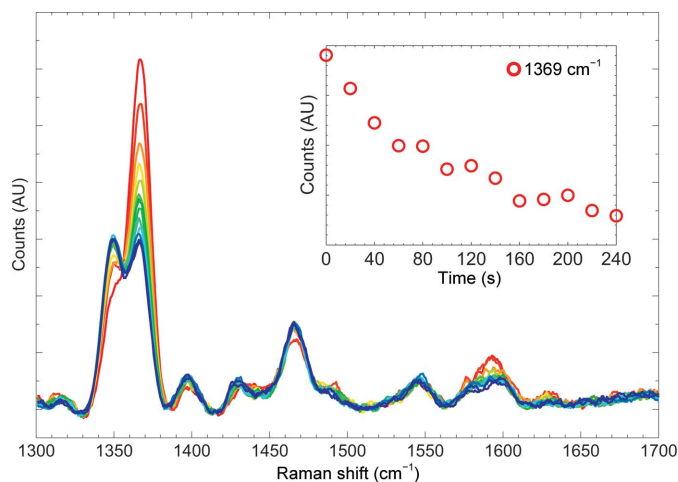
Figure 4
Consecutive resonance Raman spectra from a CO-bound crystal, each measured over 20 s of laser exposure at ~5 mW power with no X-ray exposure for a total irradiation time of 240 s. The starting (red) and final (blue) spectra are highlighted. Significant laser effects consistent with ligand dissociation were observed. Note that a degree of CO dissociation occurred even during measurement of the starting spectrum, as indicated by the shoulder in the ν_4 band at ~1350 cm^{-1} and the peak at ~1465 cm^{-1}. The inset shows the decay of the Raman band at 1369 cm^{-1} as a function of exposure time.

NO complex are 8–10 cm^{-1} higher in the crystalline state. This mirrors the trend for the ferric and ferrous states (Table 1), suggesting that the slight increases in the ν_3 and ν_{10} frequencies are a specific feature of the crystalline state. No laser-induced dissociation of bound NO was observed in our experiments and the crystal structure (Supplementary Fig. S4) was essentially identical to that described previously (Hough *et al.*, 2011). Our data are consistent with previous work where only X-ray dissociation of NO, not laser dissociation, was observed in haemoglobin crystals (Merlino *et al.*, 2013). In contrast, the AxCYTcp–CO complex was found to be highly susceptible to laser-induced ligand dissociation. At 5 mW laser power at the sample, progressive conversion from the ferrous CO spectrum to that of the ferrous 5c complex was observed in successive spectra (Fig. 4). This is consistent with, for example, flash-photolysis experiments, in which laser light at similar wavelengths can be used to dissociate CO from haem in order to investigate the kinetics of rebinding. We note here that dissociation will only be observed in the penetration depth of the laser into the crystal and thus this phenomenon, if not monitored and avoided, could cause a discrepancy between RR and crystallographic data measured on the same crystal.

4. Discussion

The combined RR and crystallographic data described here demonstrate that online RR spectroscopy is a powerful tool for fingerprinting both redox and ligand states in single crystals of haemproteins. RR spectroscopy allows information on vibrational states to be gained and, if performed on-axis, is particularly useful for large crystals, where UV–visible absorption microspectrophotometry is not feasible owing to the high optical density of the haemprotein crystals. High signal-to-noise RR spectra over the wavenumber range 600–2000 cm^{-1} were obtained from AxCYTcp crystals at 100 K using low laser powers (up to 1.95 mW) to avoid laser-induced reduction of haem or ligand dissociation. Characteristic spectra were measured for the ferric, ferrous, ferrous NO and ferrous CO states with clear resolution of the redox-marker band ν_4 and the core size marker bands ν_2, ν_3 and ν_{10}. The corresponding structures were comparable to those previously measured in crystallography-only experiments, but with an increased level of functional state reliability as a result of explicit validation of redox and ligand states.

RR data measured at 100 K from different redox and ligand states generally matched the corresponding solution data measured at the same temperature well. Some differences in frequencies occurred and this may be owing to the changes to vibrational modes imposed by the crystalline lattice. Nevertheless, ferric and ferrous states and 6c (CO) and 5c (NO) complexes were clearly distinguished using RR data, allowing these biologically relevant changes to be monitored and followed by comparison to corresponding solution data. This approach can identify mixed populations in crystals, for example of ferric/ferrous oxidation state or incomplete ligand binding, although only in the region penetrated by the laser.

RR spectra measured from crystals of ferric *Ax*CYTcp before and after X-ray exposure showed significant changes owing to the conversion of ferric to ferrous protein, with reduction occurring following an X-ray dose of only 0.19 MGy. X-ray photoreduction of haemprotein crystals has been well characterized (see, for example, Beitlich *et al.*, 2007). In the case of *Ax*CYTcp, significant structural differences in the position of a proximal pocket arginine residue were observed between structures determined from a crystal reduced by X-rays and from a crystal chemically reduced using sodium ascorbate prior to cooling, despite both having RR spectra consistent with the ferrous state. This apparent discrepancy was resolved by determination of the structures of X-ray-reduced crystals at 160 and 180 K, which contained electron density for both the 'ferric' and 'ferrous' arginine positions. Given these results, it is possible that the ferric crystals used for the determination of previous structures of *Ax*CYTcp may have undergone partial X-ray reduction of Fe, but that given the lack of conformational changes observed between the ferric and X-ray-reduced structures at 100 K this was not apparent without complementary microspectrophotometric data.

The temperature at which protein crystals undergo the formation of crystalline ice and a catastrophic loss of crystalline order varies between crystals and is influenced by the size of the solvent channels (Weik, Kryger *et al.*, 2001). In acetylcholinesterase (Weik, Kryger *et al.*, 2001) this occurred at >155 K, whereas in *Ax*CYTcp it did not occur at either 160 or 180 K. The observation of partial occupancies of two distinct Arg124 conformers in our 160 and 180 K *Ax*CYTcp structures argues that there are two distinct, energetically favourable positions for the side chain and the flip from one to the other requires a combination of sufficiently high thermal energy and sufficiently low solvent viscosity. Weik, Kryger *et al.* (2001) proposed that a solvent glass transition occurs between 100 and 155 K, with the higher temperature solvent displaying a greatly decreased viscosity that facilitates conformational changes in amino acids. Weik and coworkers have also demonstrated that product escape (Colletier *et al.*, 2008) and side-chain flexibility (Weik, Ravelli *et al.*, 2001) can be observed in structures of acetylcholinesterase measured at 155 K that were supressed at 100 K.

Elevated temperatures above 150 K but below the temperature at which crystals are damaged by crystalline ice formation may facilitate the observation of relaxed or responsive structures (Weik & Colletier, 2010). In the 160 and 180 K structures described here, in-crystal reduction by X-rays has been achieved while still maintaining crystalline order and diffracting power. The relatively lower temperature of ∼160–180 K prevents the 'destructive' level of radiation damage associated with room-temperature data collection, although more radiation damage is observed than at 100 K.

High-quality characteristic vibrational frequencies of the porphyrin marker bands were obtained for both NO-bound and CO-bound states of *Ax*CYTcp, which were consistent with the obtained crystal structures and solution data. However, care must be taken when exposing CO-bound haemprotein crystals to laser light, as this can lead to dissociation of the CO ligand at high laser powers. Previous studies have shown that in myoglobin, photo-dissociated CO was able to migrate away from haem even at 20 K (Brunori *et al.*, 2000).

Such effects are insidious as they will occur only in the part of the crystal penetrated by the laser beam and may therefore misrepresent the ligand status in the crystal as a whole. The data described here using a 405 nm solid-state excitation laser were limited to a lower wavenumber shift of ∼600 cm^{-1} owing to the notch filters used within the instrument. A number of important resonance Raman bands for Fe–CO and Fe–NO complexes lie at lower wavenumbers (∼450 and ∼579 cm^{-1}; Andrew *et al.*, 2001), and future developments in the SLS instrumentation will aim to access this important spectral region.

In conclusion, high-resolution X-ray crystallography was effectively combined with resonance Raman spectroscopy to 'fingerprint' and validate different redox and ligand states in structures of *Ax*CYTcp. This combination of techniques provides a powerful tool to solve and correctly determine the true redox and ligand states in haemprotein crystals and would be valuable as a routine experimental procedure at advanced crystallographic beamlines. The combination of online spectroscopic techniques with X-ray crystallography is particularly important in micro-focused and nano-focused facilities, where the X-ray photon density will be much higher than the original facilities at the third-generation SR sources. The whole armoury of spectroscopic probes, *e.g.* UV–Vis, RR and XAS, have a significant role to play in providing functionally validated structures of redox proteins.

References

Adar, F., Lee, E., Mamedov, S. & Whitley, A. (2010). *Microsc. Microanal.* **16**, 360–361.

Andrew, C. R., George, S. J., Lawson, D. M. & Eady, R. R. (2002). *Biochemistry*, **41**, 2353–2360.

Andrew, C. R., Green, E. L., Lawson, D. M. & Eady, R. R. (2001). *Biochemistry*, **40**, 4115–4122.

Andrew, C. R., Kemper, L. J., Busche, T. L., Tiwari, A. M., Kecskes, M. C., Stafford, J. M., Croft, L. C., Lu, S., Moënne-Loccoz, P., Huston, W., Moir, J. W. & Eady, R. R. (2005). *Biochemistry*, **44**, 8664–8672.

Antonyuk, S. V. & Hough, M. A. (2011). *Biochim. Biophys. Acta*, **1814**, 778–784.

Antonyuk, S. V., Rustage, N., Petersen, C. A., Arnst, J. L., Heyes, D. J., Sharma, R., Berry, N. G., Scrutton, N. S., Eady, R. R., Andrew, C. R. & Hasnain, S. S. (2011). *Proc. Natl Acad. Sci. USA*, **108**, 15780–15785.

Beitlich, T., Kühnel, K., Schulze-Briese, C., Shoeman, R. L. & Schlichting, I. (2007). *J. Synchrotron Rad.* **14**, 11–23.

Bourgeois, D., Katona, G., de Rosny, E. & Carpentier, P. (2009). *Methods Mol. Biol.* **544**, 253–267.

research papers

Brunori, M., Vallone, B., Cutruzzola, F., Travaglini-Allocatelli, C., Berendzen, J., Chu, K., Sweet, R. M. & Schlichting, I. (2000). *Proc. Natl Acad. Sci. USA*, **97**, 2058–2063.

Carpentier, P., Royant, A., Ohana, J. & Bourgeois, D. (2007). *J. Appl. Cryst.* **40**, 1113–1122.

Chen, V. B., Arendall, W. B., Headd, J. J., Keedy, D. A., Immormino, R. M., Kapral, G. J., Murray, L. W., Richardson, J. S. & Richardson, D. C. (2010). *Acta Cryst.* D**66**, 12–21.

Colletier, J.-P., Bourgeois, D., Sanson, B., Fournier, D., Sussman, J. L., Silman, I. & Weik, M. (2008). *Proc. Natl Acad. Sci. USA*, **105**, 11742–11747.

Daughtry, K. D., Xiao, Y., Stoner-Ma, D., Cho, E., Orville, A. M., Liu, P. & Allen, K. N. (2012). *J. Am. Chem. Soc.* **134**, 2823–2834.

Ellis, M. J., Buffey, S. G., Hough, M. A. & Hasnain, S. S. (2008). *J. Synchrotron Rad.* **15**, 433–439.

Emsley, P., Lohkamp, B., Scott, W. G. & Cowtan, K. (2010). *Acta Cryst.* D**66**, 486–501.

Evans, P. (2006). *Acta Cryst.* D**62**, 72–82.

Garton, E. M., Pixton, D. A., Petersen, C. A., Eady, R. R., Hasnain, S. S. & Andrew, C. R. (2012). *J. Am. Chem. Soc.* **134**, 1461–1463.

Henrich, B., Bergamaschi, A., Broennimann, C., Dinapoli, R., Eikenberry, E. F., Johnson, I., Kobas, M., Kraft, P., Mozzanica, A. & Schmitt, B. (2009). *Nucl. Instrum. Methods A*, **607**, 247–249.

Hough, M. A., Antonyuk, S. V., Barbieri, S., Rustage, N., McKay, A. L., Servid, A. E., Eady, R. R., Andrew, C. R. & Hasnain, S. S. (2011). *J. Mol. Biol.* **405**, 395–409.

Kabsch, W. (2010). *Acta Cryst.* D**66**, 125–132.

Katona, G., Carpentier, P., Nivière, V., Amara, P., Adam, V., Ohana, J., Tsanov, N. & Bourgeois, D. (2007). *Science*, **316**, 449–453.

Kruglik, S. G., Lambry, J. C., Cianetti, S., Martin, J. L., Eady, R. R., Andrew, C. R. & Negrerie, M. (2007). *J. Biol. Chem.* **282**, 5053–5062.

Lawson, D. M., Stevenson, C. E., Andrew, C. R. & Eady, R. R. (2000). *EMBO J.* **19**, 5661–5671.

Martin, E., Berka, V., Sharina, I. & Tsai, A. L. (2012). *Biochemistry*, **51**, 2737–2746.

Meharenna, Y. T., Doukov, T., Li, H., Soltis, S. M. & Poulos, T. L. (2010). *Biochemistry*, **49**, 2984–2986.

Merlino, A., Fuchs, M. R., Pica, A., Balsamo, A., Dworkowski, F. S. N., Pompidor, G., Mazzarella, L. & Vergara, A. (2013). *Acta Cryst.* D**69**, 137–140.

Murshudov, G. N., Skubák, P., Lebedev, A. A., Pannu, N. S., Steiner, R. A., Nicholls, R. A., Winn, M. D., Long, F. & Vagin, A. A. (2011). *Acta Cryst.* D**67**, 355–367.

Orville, A. M., Buono, R., Cowan, M., Héroux, A., Shea-McCarthy, G., Schneider, D. K., Skinner, J. M., Skinner, M. J., Stoner-Ma, D. & Sweet, R. M. (2011). *J. Synchrotron Rad.* **18**, 358–366.

Owen, R. L., Yorke, B. A., Gowdy, J. A. & Pearson, A. R. (2011). *J. Synchrotron Rad.* **18**, 367–373.

Pearson, A. R. & Owen, R. L. (2009). *Biochem. Soc. Trans.* **37**, 378–381.

Pearson, A. R., Pahl, R., Kovaleva, E. G., Davidson, V. L. & Wilmot, C. M. (2007). *J. Synchrotron Rad.* **14**, 92–98.

Pompidor, G., Dworkowski, F. S. N., Thominet, V., Schulze-Briese, C. & Fuchs, M. R. (2013). *J. Synchrotron Rad.* **20**, 765–776.

Saavedra, J. E., Southan, G. J., Davies, K. M., Lundell, A., Markou, C., Hanson, S. R., Adrie, C., Hurford, W. E., Zapol, W. M. & Keefer, L. K. (1996). *J. Med. Chem.* **39**, 4361–4365.

Silkstone, G., Kapetanaki, S. M., Husu, I., Vos, M. H. & Wilson, M. T. (2012). *Biochemistry*, **51**, 6760–6766.

Stoner-Ma, D., Skinner, J. M., Schneider, D. K., Cowan, M., Sweet, R. M. & Orville, A. M. (2011). *J. Synchrotron Rad.* **18**, 37–40.

Tsai, A. L., Berka, V., Sharina, I. & Martin, E. (2011). *J. Biol. Chem.* **286**, 43182–43192.

Weik, M. & Colletier, J.-P. (2010). *Acta Cryst.* D**66**, 437–446.

Weik, M., Kryger, G., Schreurs, A. M. M., Bouma, B., Silman, I., Sussman, J. L., Gros, P. & Kroon, J. (2001). *Acta Cryst.* D**57**, 566–573.

Weik, M., Ravelli, R. B. G., Silman, I., Sussman, J. L., Gros, P. & Kroon, J. (2001). *Protein Sci.* **10**, 1953–1961.

Winn, M. D. et al. (2011). *Acta Cryst.* D**67**, 235–242.

Zeldin, O. B., Gerstel, M. & Garman, E. F. (2013). *J. Synchrotron Rad.* **20**, 49–57.